CHEMISTRY
A EUROPEAN JOURNAL

DOI: 10.1002/chem.200600891

Effect of Core Twisting on Self-Assembly and Optical Properties of Perylene Bisimide Dyes in Solution and Columnar Liquid Crystalline Phases

Zhijian Chen,[a] Ute Baumeister,[b] Carsten Tschierske,[c] and Frank Würthner*[a]

Abstract: A series of highly soluble and fluorescent core-twisted perylene bisimide dyes (PBIs) **3a–f** with different substituents at the bay area (1,6,7,12 positions of the perylene core) were synthesized and fully characterized by ^{1}H NMR, UV/Vis spectroscopy, MS spectrometry, and elemental analysis. The π–π aggregation properties of these new functional dyes were investigated in detail both in solution and in condensed phase by UV/Vis and fluorescence spectroscopy, vapor pressure osmometry (VPO), differential scanning calorimetry (DSC), polarizing optical microscopy (POM), and X-ray diffraction. Concentration-dependent UV/Vis measurements and VPO analysis revealed that these core-twisted π-conjugated systems show distinct self-dimerization equilibria in apolar solvent methylcyclohexane (MCH) with dimerization constants between 1.3×10^4 and $30\,\text{M}^{-1}$. The photoluminescence spectra of the dimers of PBIs **3a–f** exhibit bathochromic shifts of quite different magnitude which could be attributed to different longitudinal or rotational offsets between the dyes as well as differences in the respective π–π stacking distance. In condensed state, quite a few of these PBIs form luminescent rectangular or hexagonal columnar liquid crystalline phases with low isotropization temperatures. The effects of the distortion of the π systems on their π–π stacking and the optical properties of the resultant stacks in solution and in LC phases have been explored in detail. In one case (**3a**) a particularly interesting phase change from crystalline into liquid crystalline could be observed upon annealing that was accompanied by a transformation from nonfluorescent *H*-type into strongly fluorescent *J*-type packing of the dyes.

Keywords: dyes/pigments · liquid crystals · perylene bisimide · pi–pi stacking · self-assembly

Introduction

Self-assembled π-conjugated systems have attracted tremendous attention in the past years owing to their potential application in organic electronics.[1] Numerous functional π systems, for example, triphenylenes,[2] porphyrins,[3] phthalocyanines,[4] hexabenzocoronenes,[5] and perylene bisimides (PBIs)[6] have been intensively investigated aiming to their application as optical recording media,[7] organic photoconductors,[8] semiconductors,[9] and solar cells.[10] In recent years, emphasis has been given on the organization of tailored functional π systems by self-assembly leading to one-dimensional stacks of π–π aggregates in solution,[11] in organogels,[12] and in columnar liquid crystalline (LC) phases.[13] The major interest in π–π aggregated assemblies stems from their potential applications as conductive nanowires[14] in organic electronics due to the effective π-orbital interactions among the molecules which facilitate the hopping of charge carriers.[15] At a first glance, it might be expected that charge carrier mobility should benefit from a large size planar aromatic core of the functional dyes.[16] However, in our recent studies, we have demonstrated that a high charge carrier mobility is feasible for nonplanar PBI dyes with chlorine substituents at bay area, thus, the concept of "core-twisted π systems" has been established.[17] The pronounced distortion of the π system of these dyes, which is caused by the steric encumbering effect of the substituents at bay area (1,6,7,12

[a] Z. Chen, Prof. F. Würthner
Universität Würzburg, Institut für Organische Chemie
and Röntgen Research Center for Complex Material Systems
Am Hubland, 97074 Würzburg (Germany)
Fax: (+49) 931-888-4756
E-mail: wuerthner@chemie.uni-wuerzburg.de

[b] Dr. U. Baumeister
Martin-Luther-Universität Halle-Wittenberg
Institut für Physikalische Chemie, Mühlpforte 1
06108 Halle (Germany)

[c] Prof. C. Tschierske
Martin-Luther-Universität Halle-Wittenberg
Institut für Organische Chemie, Kurt-Mothes Strasse 2
06120 Halle (Germany)

Supporting information for this article is available on the WWW under http://www.chemeurj.org/ or from the author: Additional UV/Vis, fluorescence, VPO, DSC, X-ray diffraction data, and other measurements of the PBI dyes.

positions in the perylene core), leads to a unique two-dimensional organization of the molecules in the solid state with close contacts that is not available for the planar unsubstituted PBI dyes. This contact pattern facilitates the charge transport and leads to an isotropic charge carrier mobility up to 0.14 $cm^2V^{-1}s^{-1}$ as revealed by pulse radiolysis-time resolved microwave conductivity[17] measurements. More recently, Nuckolls and co-workers have reported another example, that is, a contorted hexabenzocoronene system, which exhibits a field-effect transistor (FET) mobility of 0.02 $cm^2V^{-1}s^{-1}$.[18] These studies have shown that core-twisted π-conjugated discotic systems are of great interest for the exploration of new organic electronic materials. In this regard core-twisted PBIs are particularly promising as PBIs are among the best n-type organic semiconductors to date.[19] In comparison with planar unsubstituted PBI dyes, contorted derivatives exhibit in general much higher solubility and significantly lower isotropization points (up to 190 °C lower than the unsubstituted PBIs (see below) that are favorable properties for the fabrication of electronic devices.[20]

Herein, we report the synthesis of a series of new, core-twisted PBI dyes containing tridodecylphenyl substituents at the imide positions and various substituents at bay area. The advantage of the tridodecylphenyl substituents is that the fluorescence quantum yield can be largely improved in comparison with the analogue dyes bearing the alkyloxyphenyl substituents[21] without losing valuable self-assembly properties such as the liquid crystallinity of the compounds. The self-assembly and optical properties of the present PBI dyes in solution and liquid crystal phase have been investigated by UV/Vis and fluorescence spectroscopy, vapor pressure osmometry (VPO), polarizing optical microscopy (POM), differential scanning calorimetry (DSC) and X-ray diffraction. Furthermore, the effect of core twisting on the self-assembly and optical properties of π–π stacks of these functional dyes is discussed in detail.

Results

Synthesis: The *N*,*N*′-di(tridodecylphenyl)-substituted perylene bisimides (PBIs) **3a–d** were synthesized by condensation of the respective perylene tetracarboxylic bisanhydrides (PBAs) **1a–d** bearing different types of bay substituents with 3,4,5-tridodecylaniline (**2**)[22] according to Scheme 1. We have previously reported that direct bromination of unsubstituted PBA affords a regioisomeric mixture of 1,6- and 1,7-dibromo PBA in a ratio of about 1:4.[23] Since these isomers possess similar reactivity, their subsequent reaction leads to regioisomeric product mixtures that are often difficult to purify by silica gel column chromatography. We could overcome this problem by repeated recrystallization of the regioisomeric mixture of compound **4** (see below) to obtain the isomer-free 1,7-dibrominated product as precursor for further regioisomerically pure 1,7-disubstituted PBIs.[23] Thus, the saponification of **4** gave isomerically pure 1,7-dibrominated PBA **1d** (verified by 600 MHz ^{1}H NMR), which condensed with aniline **2** to afford 1,7-dibrominated PBI **3d** (Scheme 1). The subsequent nucleophilic substitution of the bromine atoms in **3d** by appropriate phenol derivatives afforded the corresponding isomer-free dyes **3e** and **f**. Similarly, the nucleophilic reaction of 1,7-dibrominated PBI **4** with pyrrolidine gave the corresponding 1,7-dipyrrolidinyl PBI derivative, which was subsequently hydrolyzed to afford the pyrrolidinyl-substituted PBA **1c**. The imidization of the latter bisanhydride with **2** afforded **3c**. The PBIs **3a–f** are fully characterized by ^{1}H NMR, UV/Vis, fluorescence spectroscopy, MS spectrometry, and elemental analysis.

Optical properties of bay-substituted PBI monomers: The optical properties of **3a–f** were investigated by UV/Vis and fluorescence spectroscopy. The absorption spectra of these dyes in CH_2Cl_2 are depicted in Figure 1 and the optical data are summarized in Table 1. These dyes show broad S_0–S_1 absorption bands with absorption maxima in the range of 524–

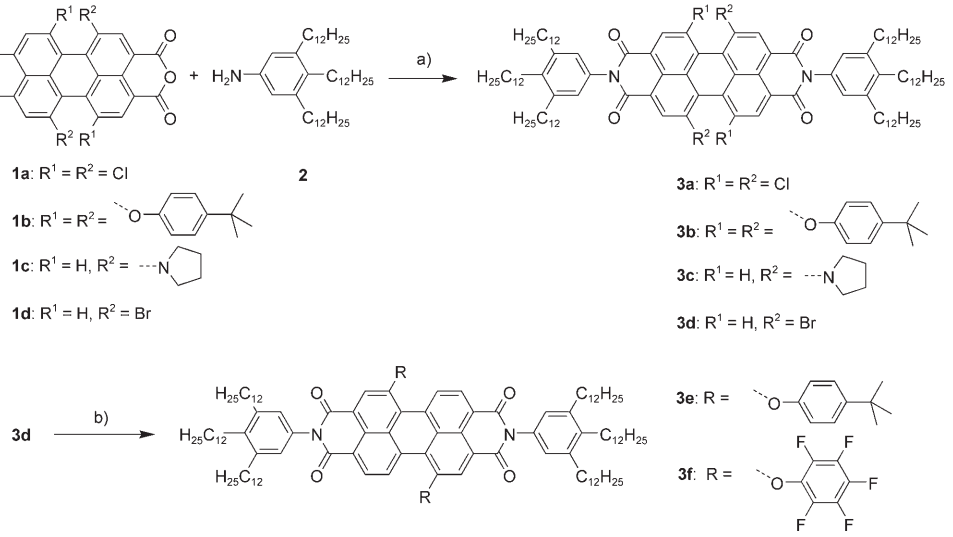

Scheme 1. Synthesis of PBIs **3a–f**: a) $Zn(OAc)_2$, quinoline, 180 °C, 3 h, yields: 52 % (**3a**), 53 % (**3b**), 65 % (**3c**), and 44 % (**3d**); b) *p*-*tert*-butylphenol (for **3e**) or pentafluorophenol (for **3f**), K_2CO_3, *N*-methyl-2-pyrrolidone (NMP), 120 °C, 2 h, yields: 40 % (**3e**), and 61 % (**3f**).

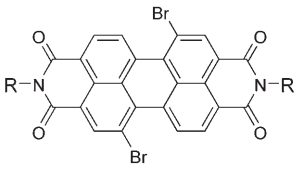

4: R =

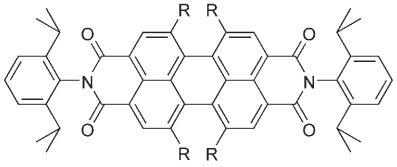

5: R =

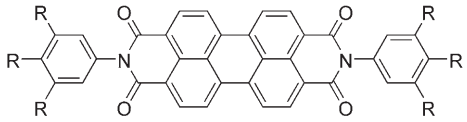

6: R = *n*-$C_{12}H_{25}$

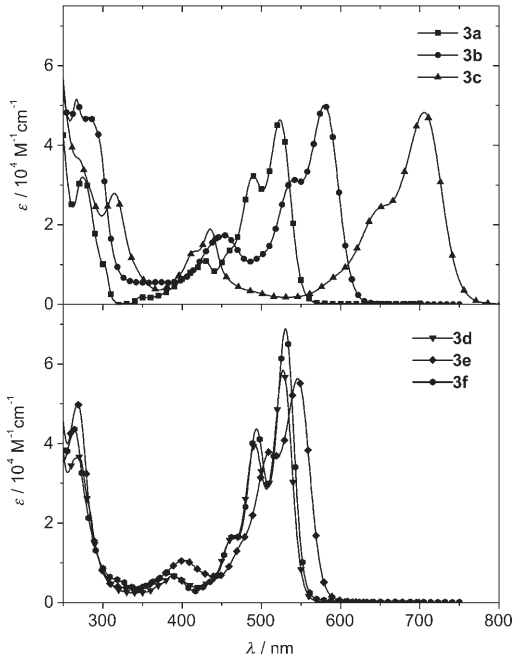

Figure 1. UV/Vis absorption spectra of dyes **3a–f** in CH_2Cl_2.

Table 1. Optical properties of PBIs **3a–f** in CH_2Cl_2.

Compound	λ_{abs} [nm]	ε_{max} [$M^{-1}cm^{-1}$]	λ_{em} [nm]	Φ_{fl}
3a	524	48100	543	0.03
3b	580	50100	611	0.95
3c	705	48200	745	0.25
3d	527	57800	544	0.26
3e	546	56000	575	0.87
3f	530	71300	547	0.79

705 nm. Depending on their λ_{abs}, the solutions of these dyes exhibit various colors from orange (**3a**) to deep green (**3c**). The absorption maxima of the PBI derivatives, which contain electron-withdrawing substituents such as Cl (**3a**), Br (**3d**), or pentafluorophenoxy groups (**3f**) at the bay positions are only slightly shifted with respect to that of the unsubstituted reference PBI **6** (see preceding paper, λ_{abs} = 527 nm in CH_2Cl_2).[22] But, for PBI derivatives with electron-donating groups a large bathochromic shift of λ_{abs} was observed relative to the unsubstituted PBI **6** (56 nm for **3b**, 181 nm for **3c**, 22 nm for **3e**), reflecting pronounced electronic interactions between the perylene bisimide core and the electron-donating groups in bay area. The absorption spectra of these dyes displayed vibronic structures in the S_0-S_1 absorption bands,[24] indicating that the electronic transition is coupled with the vibration of the perylene skeleton. In comparison with the spectrum of unsubstituted PBI **6**, the lineshape of the spectra for the bay-substituted dyes **3a–f** are broader and display less vibronic structures due to the loss of planarity of the perylene core and the lower molecular symmetry caused by the bay substituents. (Several X-ray crystal structures of bay-substituted PBIs revealed a significant distortion of the perylene skeleton). For all these dyes, a second absorption band was observed at around 400 nm that can be attributed to the transition from the ground state to a higher excited state.[24] Previously, it was pointed out that the S_0–S_2 transition is symmetry forbidden for unsubstituted PBIs.[24b] However, due to the twisted nature and lower symmetry of the present bay-substituted PBIs such transition is not strictly forbidden, thus the apparent absorption coefficients of these bands were increased in comparison with that of unsubstituted PBIs.

All of these dyes **3a–f** are photoluminescent as their fluorescence spectra in CH_2Cl_2 revealed (Figure 2). The emission bands of these compounds are approximately the mirror image of their S_0–S_1 absorption bands with Stokes shift between 17 and 40 nm (corresponding to 590 to 760 cm^{-1} in wavenumbers). The emission maxima (λ_{em}) of the bay-substituted PBIs **3a–f** depend on the electronic properties of the bay substituents. For **3a** and **d** with electron-withdrawing halogen atoms λ_{em} at 524 and 544 nm, respectively, were observed, while the dye **3c** with two electron-donating pyrrolidine groups showed λ_{em} at 745 nm. As expected, from our previous work on **6**[22a] the fluorescence quantum yields (Φ_{fl}) of dyes **3b** (0.95) and **3e** (0.87) are greatly improved in comparison with those of analogous dyes bearing trialkoxyphenyl groups, instead of trialkylphenyl groups, at the imide positions (Φ_{fl} = 0.23).[21] While for these phenoxy-substituted compounds **3b**, **e** and **f** high Φ_{fl} values (0.79–0.95) were observed, the halogen-containing derivatives **3a** and **d** exhibit relatively low fluorescence quantum yield (Table 1) that may be attributed to fluorescence quenching by photoinduced electron transfer processes. In accordance with this assumption, the quantum yield of the dyes **3a** and **3d** is significantly improved from 0.03 and 0.26, respectively, in polar solvent CH_2Cl_2 to 0.37 and 0.67, respectively, in apolar methylcyclohexane (MCH).

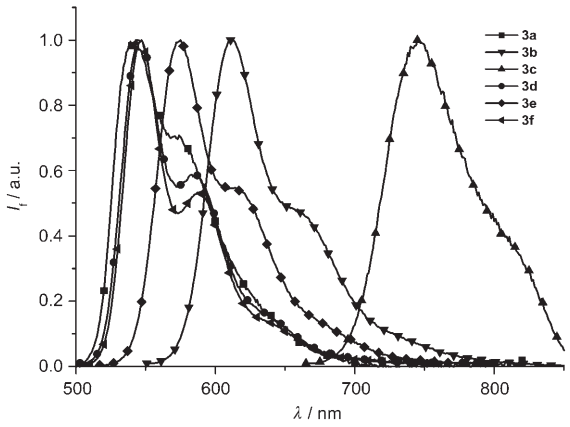

Figure 2. Normalized steady-state fluorescence spectra of compounds **3a–f** in CH_2Cl_2.

Formation of π–π-stacked dimers of PBIs and their photoluminescence properties in solutions: The aggregation behavior of PBIs **3a–f** was investigated by concentration-dependent UV/Vis spectroscopy in MCH. Upon increasing the concentration of the dyes pronounced spectral changes, including hypochromism (decrease of the apparent absorption coefficients) and shifts of the absorption peaks were observed (Figure 3 and Figures S1–2 in the Supporting Information), which clearly indicate the formation of aggregates in this apolar solvent. For all these dyes, a broadening of the spectra and a loss of the fine structures were observed upon aggregation. Interestingly, dyes **3a** and **3b** showed a bathochromic shift of the absorption maximum (5 nm for **3a** and 10 nm for **3b**), while a hypsochromic shift of the absorption maximum was observed for the remaining dyes (41 nm for **3c**, 34 nm for **3d**, 27 nm for **3e** and 32 nm for **3f**). Such shifts of absorption maxima imply the formation of *J*-type or *H*-type excitonic coupling regimes in these aggregates (see Discussion).

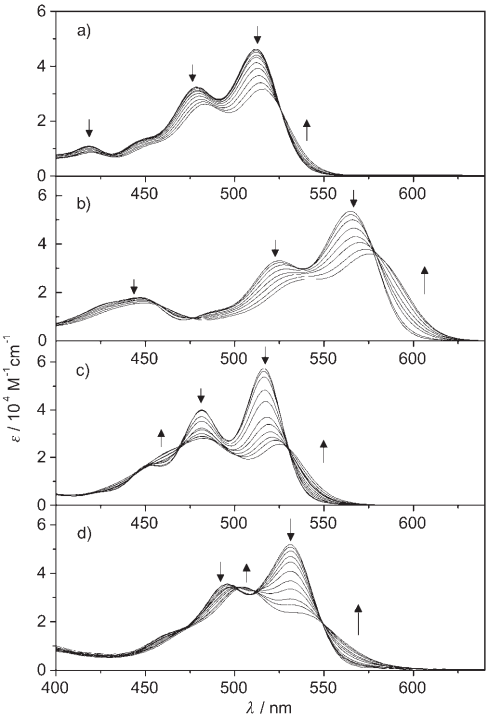

Figure 3. Concentration-dependent UV/Vis spectra in MCH for a) **3a** (5.2×10^{-6} to 7.7×10^{-2} M); b) **3b** (2.2×10^{-6} to 1.2×10^{-2} M); c) **3d** (5.1×10^{-6} to 1.4×10^{-2} M); and d) **3e** (5.1×10^{-7} to 2.6×10^{-3} M). The arrows indicate the spectral changes upon increasing concentration.

However, only from the UV/Vis spectral data it cannot be assessed whether dimer or higher aggregates prevail.[25] Therefore, vapor pressure osmometry (VPO) was employed to determine the size of the aggregated species of the present PBIs. For the reference PBI **5** (structure see above) containing very bulky substituents, the obtained colligative concentrations were identical with the stoichiometric concentration of the MCH stock solution, indicating that this compound does not aggregate in the concentration range applied. VPO measurements for dye **3d** were performed at 5 different concentrations in the range of 0.0016 to 0.0132 molal (about 0.0013 to 0.0104 M) and a reduction of the colligative concentrations to about half of that for **5** was observed (Figure S3 in the Supporting Information). Based on the measured colligative concentrations, the aggregation numbers *N* of this dye were calculated as 1.3 to 1.7 at different concentrations. For the remaining dyes **3a–c** and **e**,**f**, *N* values between 1.1 and 1.8 were obtained. These results are in compliance with a dimerization process in the given range of concentration for the present bay-substituted PBIs in MCH. The smaller *N* values observed for **3a** and **b** (1.1 and 1.4, respectively) can be attributed to the relatively small dimerization constants (see Table 2) of these dyes and the coexistence of dimers and a large amount of monomeric species at the measured concentration. For comparison, in the case of planar PBI dye **6** the formation of oligomeric stacks $N > 5$ was observed,[22] underlining the significant difference in π–π aggregation properties of the planar and distorted PBI dyes.

By nonlinear regression analysis of the UV/Vis spectral data with the dimer aggregation model, which has been successfully used for other dyes,[26] the dimerization constants (K_D) and the Gibbs free energy changes (ΔG°) at 298 K were determined. The results are summarized in Table 2 and a plot of the molar fraction of dimerized dyes α_{dimer} at different concentrations is depicted in Figure 4. The curves calculated from the dimer model fit very well with the experimental data points. For compound **3e** and **f** with two phenoxy and pentafluorophenoxy bay substituents, respectively,

Table 2. Dimerization constants and corresponding Gibbs free energy changes at 298 K for the dyes **3a–f** in MCH.

Compound	K_D [L mol^{-1}]	$-\Delta G^\circ_{298}$ [kJ mol^{-1}]
3a	30	8.4
3b	9.1×10^2	16.9
3c	1.3×10^4	23.5
3d	4.6×10^3	20.9
3e	7.9×10^3	22.2
3f	7.3×10^3	22.0

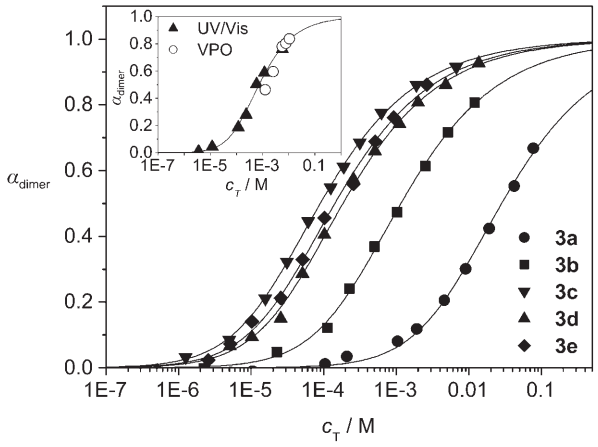

Figure 4. Plot of the molar fraction of the dimerized molecules α_{dimer} versus the total concentration c_T of the dyes **3a**–**e** obtained from the concentration-dependent UV/Vis spectral data in MCH at 25 °C (for clarity, the curve and data points of **3f** are not shown since they completely overlap with those of **3e**). Inset: α_{dimer} of compound **3d** as a function of c_T obtained from concentration-dependent UV/Vis spectroscopy (triangles) and VPO (circles) at 44 °C.

nearly identical K_D values were observed. It is noteworthy that for **3b** and **e** the aggregation constants are about two orders of magnitude smaller than those previously observed for PBIs containing the same substituents at bay positions, but more electron-rich tridodecyloxyphenyl substituents at imide positions.[21] Apparently, in the case of tridodecyloxyphenyl-substituted PBIs either better stacking or additional donor-acceptor interactions are provided by the more electron-rich alkoxy groups and the electron-deficient perylene units, which lead to a stronger binding between the chromophores.[27] Thus, for such compounds much larger aggregation constants were observed.

For a better comparison of the results obtained from UV/Vis spectroscopy and VPO, the K_D of **3d** was additionally determined at 44 °C (the temperature for VPO experiments) by UV/Vis spectroscopy as a representative example and a K_D value of 1200 M^{-1} was obtained (Figure 4, inset and Figure S4 in the Supporting Information). On the other hand, K_D can be estimated at a single concentration with the equation $K_D = (1-\Phi)/c_T(2\Phi-1)^2$ for dimerization equilibrium, where Φ is the osmotic coefficient and equals to the reciprocal of the average aggregation number N.[26a] Based on the N values obtained from the VPO measurements for **3d**, K_D values in a range of 670–1600 M^{-1} were estimated at five different concentrations (Table S1 in the Supporting Information). These values are in good agreement with that obtained from UV/Vis spectroscopic data. The molar fraction of dimerized molecules α_{dimer} can be calculated from the VPO results as $\alpha_{dimer} = 2-2/N$ and the data points fit well with the curve obtained from UV/Vis spectroscopic measurements (Figure 4, inset).

The photoluminescence properties of dyes **3a**–**f** upon dimerization were studied by steady-state fluorescence spectroscopy. The fluorescence spectra of the tetrasubstituted dyes **3a** and **b** at high concentrations in MCH resemble the mirror image of the corresponding UV/Vis absorption spectra (Figure 5 and Figure S5 in the Supporting Information). These spectra show comparable lineshape as those of the monomer emission spectra and small bathochromic shifts

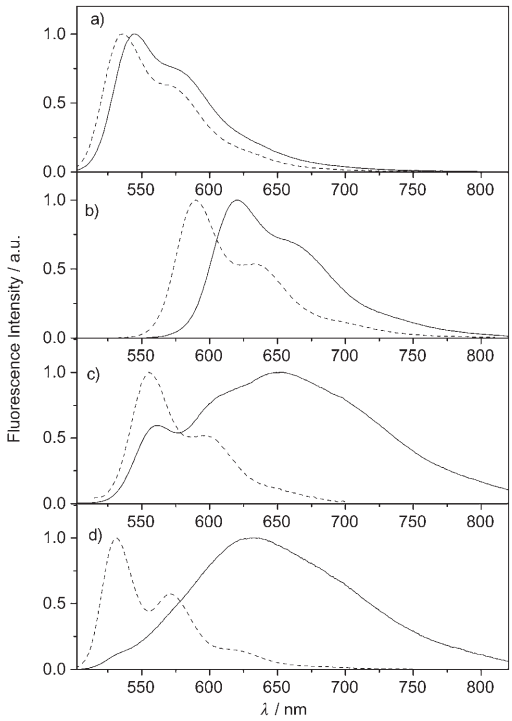

Figure 5. Normalized fluorescence spectra in MCH for a) **3a** (at 1.0×10^{-6} and 1.4×10^{-2} M); b) **3b** (at 1.0×10^{-6} and 1.0×10^{-2} M); c) **3e** (at 2.0×10^{-6} and 1.0×10^{-3} M); and d) **3f** (at 1.0×10^{-6} and 1.0×10^{-2} M). In all cases, a dashed line is used for the lower concentration and a solid line for the higher concentration.

for the 0–0 bands (9 nm for **3a** and 31 nm for **3b**). Unlike the persistent spectral profiles of the tetrasubstituted dyes, significant changes of the fluorescence spectra were observed for disubstituted **3c**–**f** upon dimerization. For **3c**, an obviously raised band was observed at around 750 nm together with the monomer emission band. The emission maximum of **3d** was bathochromically shifted from 532 to 569 nm with the loss of fine structure and significant broadening of the spectrum. More significantly, the emission spectra of **3e**,**f** displayed new, broad and unstructured bands with bathochromic shifts of about 100 nm for both dyes (2700 cm^{-1} for **3e** and 3000 cm^{-1} for **3f**). These spectral features are similar to those observed previously for aggregates of dye **6**[22] and can be related to a pronounced structural and energetical relaxation process of the excited dimer aggregate.[28]

For the two strongly photoluminescent dyes **3b** and **e** (Table 1), the change of the quantum yields upon dimerization was evaluated. The fluorescence spectra of the non-aggregated dye **5** ($\Phi_{fl} \approx 1$) and **3b** were measured at the same concentration (1.0×10^{-2} M, $\alpha_{dimer}=0.8$ for **3b**) and optical setup. The integrated fluorescence intensity (area under the

spectra) of **3b** amounts to 92% of that of **5** (after calibration by using different absorption coefficients at excitation wavelengths for **5** and **3b**). This result confirms that for **3b** the fluorescence quenching upon aggregation is negligible, which closely resembles the observation made for an analogue of PBI **3b** that contains trialkoxyphenyl groups at imide positions.[21] In contrast to that of **3b**, the fluorescence of **3e** is drastically quenched upon aggregation. Comparison of the spectra of **3e** and **5** measured under the same conditions (1.0×10^{-3} M, $\alpha_{dimer}=0.8$ for **3e**), the fluorescence quantum yield of **3e** is reduced from 0.87 (Table 1) for the monomer to only $\approx$0.19 upon aggregation. Based on these data and taking into account about 80% of **3e** is dimerized in 1.0×10^{-3} M solution, a fluorescence quantum yield of 0.02 can be calculated for the dimeric species. The shape-persistent and nondiminished fluorescence of **3b** on aggregation, on one hand, and the drastically quenched fluorescence of **3e** with large Stokes shift and unstructured new band, on the other hand, imply different stacking and relaxation modes of these dyes in their aggregates (see Discussion).

Formation and optical properties of columnar liquid crystalline phases: The combination of large-sized aromatic cores and flexible long alkyl chains has a strong effect on the self-organization properties of bulk materials and may lead to the formation of columnar liquid crystalline (LC) phases due to the anisometric shape of the molecules and microsegregation of alkyl chains and aromatic cores.[29] The thermotropic behavior of the PBI dyes **3a–f** was studied by differential scanning calorimetry (DSC), polarizing optical microscopy (POM), and X-ray diffraction (XRD). These studies revealed that the halogen- and 4-*tert*-butylphenoxy-substituted dyes **3a**, **b**, **d**, and **e** form liquid crystalline mesophases upon cooling from the melt, while only formation of an isotropic glass was observed for compounds **3c** and **f** with pyrrolidine and pentafluorophenoxy substituents, respectively. The 4-*tert*-butylphenoxy-substituted dyes **3b** and **e** were isolated as viscous birefringent substances in contrast to the halogen-substituted compounds **3a** and **d** which are crystalline at room temperature. Only one reversible transition from the birefringent phase to the isotropic liquid phase was observed for the phenoxy-substituted dyes **3b** and **e** (see Figure 6b,d), indicating that only one LC phase is formed and that there is no crystallization or only a very slow crystallization of these mesophases. The DSC heating and cooling curves of the dibromo-substituted compound **3d** are different (Figure 6c). For this compound, in addition to a small peak corresponding to the transition from the LC to the isotropic liquid state at 160°C ($\Delta H=2.7$ kJ mol^{-1}), several overlapping endothermic transitions were observed in the first heating cycle around 80°C between the pristine crystalline phase and the LC phase ($\Sigma\Delta H=127$ kJ mol^{-1}). Broad transitions with similar enthalpy changes at the same temperature range were previously reported for other liquid crystalline PBIs.[17b] No subsequent recrystallization was observed for the LC phases of the present PBIs at the employed cooling rate and exclusively the Iso-to-LC transition

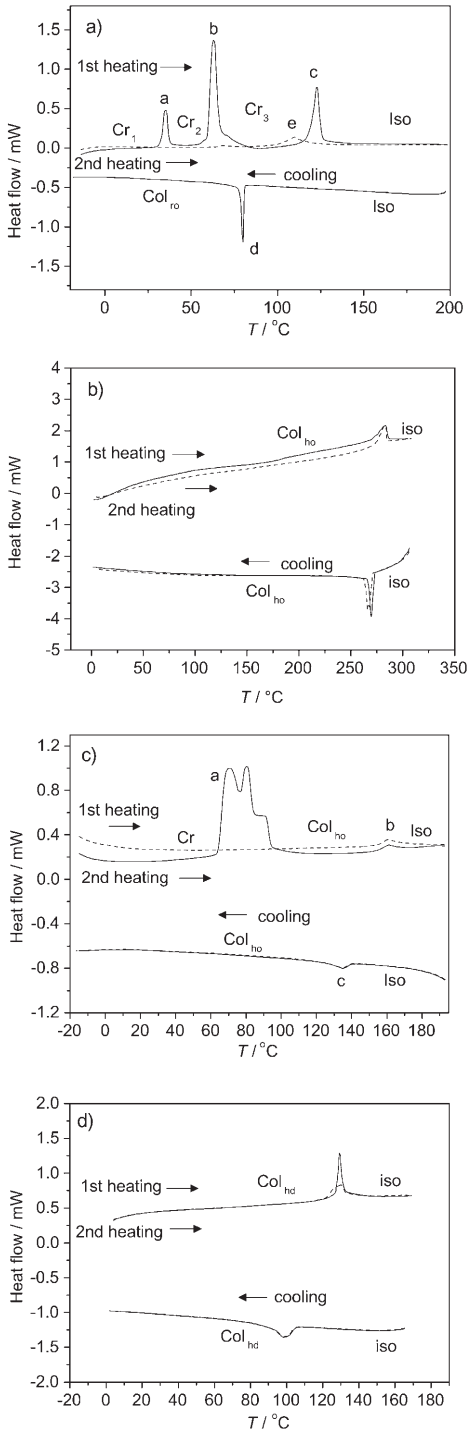

Figure 6. DSC curves (10°C min^{-1}) obtained for a) **3a**, b) **3b**, c) **3d** and d) **3e** for the first heating-cooling cycle (solid lines) and the second cycle (dashed lines).

is seen in the second and following heating curves. The most complex DSC thermogram was observed for the tetrachloro compound **3a** (Figure 6a) which showed upon first heating two crystal–crystal transitions, prior to the melting transition at 110°C. No corresponding transitions occurred in the following cooling and heating scans. Upon cooling a quite

sharp transition occurs at 80 °C, whereas the second and all following heating scans are characterized by a rather broad transition at 105 °C. This indicates a supercooling, which is often observed for columnar mesophases of relatively large disc-like mesogens and a rather high degree of intracolumnar order.

The thermodynamic properties of the LC phases of compounds **3a**, **3b**, **3d**, and **3e** are summarized in Table 3. The entropy and enthalpy changes associated with the mesophase to isotropic transitions of the disubstituted compounds **3d** and **3e** are much lower compared with those of the tetrasubstituted compounds **3a** and **3b** bearing similar substituents. For instance, the ΔH value of the dibromo-substituted compound **3d** is about one third of that for the tetrachloro-substituted compound **3a** and the ratio of ΔH for the diphenoxy- (**3e**) and tetraphenoxy-substituted (**3b**) compounds is about 1:4. A similar trend was observed for the ΔS values, which hints at a higher degree of order in the mesophases of the tetrasubstituted compounds **3a** and **b** compared with the disubstituted dyes **3d** and **e**.

Table 3. Clearing temperature T, transition enthalpies ΔH, and entropies ΔS for the LC-isotropic transitions.

Compound	Mesophase	$T_{LC\text{-}Iso}$ [°C]	ΔH [kJ mol^{-1}]	ΔS [J mol^{-1} K^{-1}]
3a	Col_{ro}	110	8.4	21.9
3b	Col_{ho}	285	23.5	42.1
3d	Col_{ho}	160	2.7	6.2
3e	Col_{hd}	130	5.3	13.2

Figure 7. Optical textures of the liquid crystalline phases of a, b) **3a** at 70 °C; c, d) **3b** at 250 °C; e) **3d** at 110 °C and f) **3e** at 105 °C as seen between crossed polarizers (the directions of polarizer and analyzer is shown by the arrows in f); a, c, e, f) show the textures obtained after slow cooling from the isotropic liquid, b, d) show the textures obtained after shearing the samples a) and c), respectively. Image size: 0.86 mm × 0.65 mm for a), b) and e)–f), 0.53 mm × 0.40 mm for c).

For these two groups of materials, there are also significant differences in the textures of the mesophases seen under a polarizing microscope between crossed polarizers. The two disubstituted compounds **3d** and **e** display spherulitic textures that are very typical for columnar LC phases (Figure 7e,f). Extinction crosses parallel to polarizer and analyzer were observed which implies that the columns in the domains are parallel to the substrate and bend into circles around the brush center.[30] The position of the extinction brushes indicates that there is no uniform tilt of the aromatic cores within the columns.

In contrast, for the tetrasubstituted compounds **3a** and **b** the formation of lancet-like domains was observed (Figure 7a,c), which reflect a certain rigidity of the columns. However, for both compounds also some spherulites coexist with the lancet-like domains (see for example Figure 7c), indicating that bending of the columns is still possible. Also in these spherulites the extinction crosses are parallel to polarizer and analyzer, again indicating the absence of a uniform tilt. In all cases shearing of the samples is possible and this gives rise to complete removal of the well-developed textures, which are replaced by nonspecific highly birefringent and nearly homogeneously aligned textures (columns predominately parallel to the substrate), as shown in Figure 7b and d for compounds **3a** and **b**, respectively. This clearly indicates the fluid liquid crystalline character of the mesophases of all four compounds.

More detailed information were obtained from X-ray diffraction measurements, which were performed for bulk samples of compounds **3a**, **b**, **d**, and **e** in the temperature regions of their mesophases.

The Guinier powder pattern of the diphenoxy-substituted compound **3e** at 80 °C shows two reflections with a ratio of the d values of $1:1/3^{1/2}$ (see Table S2 in the Supporting Information) indicating a hexagonal two-dimensional lattice. In the wide angle region, there is a diffuse scattering, revealing the fluid liquid crystalline state of the mesophase. Hence, the phase can be assigned as hexagonal columnar LC phase with only short-range order of the molecules along the stacks (Col_{hd} phase).

For the tetraphenoxy-substituted dye **3b**, the three reflections in the small angle region have a ratio of the reciprocal d spacings of $1:3^{1/2}:2$ which have been indexed as the 10, 11, and 20 reflections of a two-dimensional hexagonal lattice (Guinier powder pattern at 150 °C, see Table S2 in the Supporting Information). As for **3e**, the wide angle region is characterized by a diffuse scattering, but in this case an additional rather sharp reflection can be observed, which could be attributed to a periodic intracolumnar distance of the molecules along the stacking direction. This stacking period of $d = 0.45$ nm is identical with that for the analogous PBI dye with tridodecyloxylphenyl groups at the imide positions.[21] Hence, the LC phase at this temperature can be assigned as Col_{ho}.

A similar phase assignment results from the Guinier powder pattern and the 2D images of the scattering of an aligned sample of the dibromo-substituted dye **3d** (Col_{ho} phase, see Figure 8a,b). The *d* value for the outer sharp reflection of 0.38 nm is considerably smaller than that seen for the tetrasubstituted compound **3b**. This is reasonable, because there are only two bromine atoms in the bay positions which should allow a denser packing of the perylene cores than the four more bulky *tert*-butylphenoxy groups in compound **3b**. The 2D diffraction patterns of partially aligned samples are shown in Figure 8a,b. In this case the alignment was achieved by slow cooling of a small droplet of the material on a glass substrate. The X-ray beam was applied parallel to the substrate surface. In both samples the columns are aligned on the substrate with their long axes parallel to the substrate, whereas the direction of the X-ray beam with respect to the majority of the columns is different in Figure 8a and b. In the diffraction pattern shown in Figure 8a, the X-ray beam is nearly parallel to the long axes of most of the columns and in this alignment the hexagonal lattice is seen. In the diffraction pattern 8b, the columns are predominately perpendicular to the X-ray beam (the columns are nearly horizontal, but slightly inclined). In this diffraction pattern the rather sharp reflections at $d=0.38$ nm are seen as lines parallel to the meridian, located on the equator (see also the χ scan along the equator in Figure S6a in the Supporting Information). This proofs that the scattering at $d=0.38$ nm is due to a repeat distance within the columns (π–π stacking) and that the molecules adopt a non-tilted organization within the columns. The elongation of the reflections perpendicular to the equator shows, that there is no correlation of this intracolumnar stacking between the columns, that is, there are arbitrary displacements along the long axes of neighboring columns or they can freely shift with respect to each other along their long axes.[31]

The X-ray diffraction pattern of the tetrachloro compound **3a** is different from those of the other compounds and more complex. Figure 8c shows the diffraction pattern for a sample at 90 °C as obtained upon cooling from the isotropic phase. The five Bragg reflections observed in the small angle region can be indexed according to a two-dimensional centered rectangular lattice (*c2mm*) with satisfactory accuracy (Table S2 in the Supporting Information).[32] In the wide angle region, there are two diffuse scatterings and one more sharp scattering. The comparatively sharp peak at $2\theta=21°$ (peak b) is indicative of a periodicity in the structure with a repeat distance of 0.43 nm. Since only powder-like samples have been investigated, no direct prove could be obtained from the X-ray measurements for the direction of this periodicity within the structure. However, the *d* value of 0.43 nm is characteristic for a close contact of the π systems in perylene derivatives[17b] and this can be taken as a hint to a columnar phase with the perylene cores periodically packed along the columnar axis. Interestingly, beside the diffuse halo at $2\theta=18°$ which could be attributed to "liquid-like" disordered alkyl chains, there is a second diffuse halo at $2\theta \approx 26°$ (as a rough estimate, see Figure 8c, maximum c), corresponding to a *d* value of about 0.34 nm. To our best understanding, this unusual diffraction could be attributed to Cl–Cl close contacts in the stacks.[33] Taking the repeat distance of the perylene cores along the columnar axis ($d=0.43$ nm) as the *c* axes of a three-dimensional orthorhombic unit cell (Table 4), its volume can be calculated to $V_u=5.8$ nm^3. The volume of one molecule in the packing

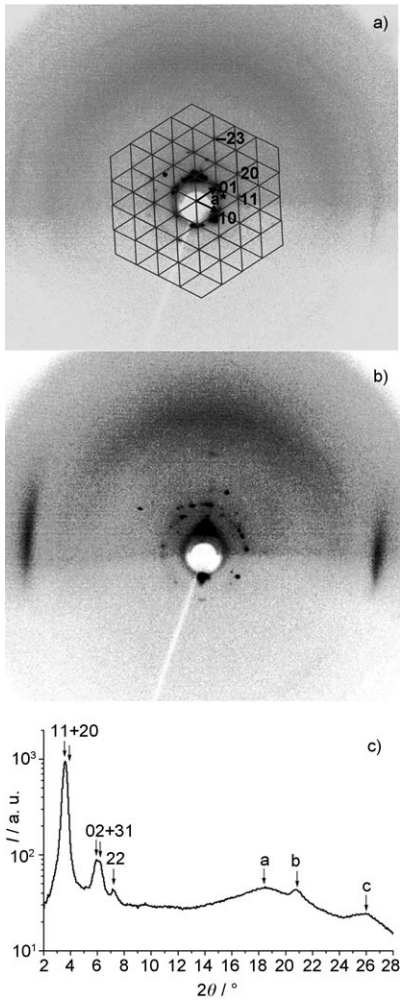

Figure 8. X-ray diffraction patterns a) of a surface-aligned sample of **3d** at 140 °C (X-ray beam parallel to the columns) showing the hexagonal lattice in the small angle region with indices of the observed reflections; b) of a partially surface-aligned sample of **3d** at 140 °C with X-ray beam perpendicular to most of the columns showing the intracolumnar stacking (for χ scans, see Figure S6a,b in the Supporting Information);[31] c) for compound **3a** at 90 °C showing the Miller indices of the small-angle reflections and the maxima of the wide-angle scattering (a, b, and c).

Table 4. LC phases, measured temperature and the corresponding lattice parameters *a* and *b*, and the repeat distance along the columns *c*.

Compound	LC phase	*T* [°C]	Lattice parameters [nm]		
			a	*b*	*c*
3a	Col_{ro}	90	4.59	2.92	0.43
3b	Col_{ho}	150	3.20		0.45
3d	Col_{ho}	140	3.02		0.38
3e	Col_{hd}	80	3.04		

has been estimated according to Immirzi et al.[34] and amounts to 2.6 nm^3. Accordingly, there should be about two molecules in the unit cell, supporting the assumption of a centered lattice. According to these XRD data, the mesophase of compound **3a** is assigned as Col_{ro}.

The unit cell parameters of the columnar LC phases of all four mesogenic compounds are summarized in Table 4. For the hexagonal columnar phases of compounds **3b**, **d**, and **e** the diameter of the columns (corresponds to a_{hex}) are 3.2, 3.0, and 3.0 nm, respectively. These diameters are significantly shorter than the long molecular axes (about 5 nm) of the dyes bearing alkyl chains in their fully extended all-*trans* conformation. The difference could be attributed to folding and interdigitation of the alkyl chains as well as rotational offsets along the stacking axis of the dyes.[22,35] This leads to an in average circular cross section of the columns which gives rise to the packing in a hexagonal lattice. Only the tetrachloro-substituted dye **3a** shows a rectangular columnar phase with a *c2mm* lattice, which can be regarded as a slightly distorted hexagonal lattice (the average diameter of the columns is also about 3.0 nm). In the case of disc-like molecules, the formation of a rectangular columnar phase is often associated with a tilted organization of the disc-like cores in the columns, which gives rise to an elliptical shape of the column cross section. For the PBI **3a**, however, there is no indication of a tilted organization of the perylene cores (see discussion of the optical textures). Moreover, the perylene core of compound **3a** itself is not disc-like, but it has a twisted conformation (see Discussion), so that an additional tilt of these cores within the columns is not very likely. It is more reasonable to assume that the distortion might arise from the restricted rotational disorder of the perylene cores due to the strong twist in the core (see Discussion). The close Cl–Cl interactions along the columns are possible also due to the segregation of these halogen regions from the regions of the flexible alkyl chains. This means that the rotational disorder of the twisted board-like PBIs around the column axis is reduced.

There are also clear differences in the X-ray wide angle scattering for the diphenoxy-substituted dye **3e**, on one hand, and compounds **3a**, **b**, and **d** on the other. PBI **3e** shows only a broad diffuse scattering (Col_{hd}), whereas for the other three compounds a much narrower peak is superimposed. This indicates that for compounds **3a**, **b**, and **d** there is a periodicity (with medium-range correlation) caused by the interaction of the π systems. The appearance of the comparatively sharp reflection at about 0.45 Å is the criterion used for the assignment of these phases as Col_{ho} and Col_{ro}. However, it should be pointed out that in general there is no distinct transition between Col_{ho} and Col_{hd} phases. Instead, there is a continuous increase of the correlation length of the periodicity within the columns. In the Col_{ho}/Col_{ro} phases of the compounds reported herein, the full width at half maximum (FWHM) is still rather large, thus the correlation length should not exceed a few molecules. A rough estimate for the correlation length in the case of **3d** may be calculated from the FWHM value Δq of the peak on the equator of the pattern in Figure 8b ($\Delta q = 0.98\ nm^{-1}$, see Figure S6c, Supporting Information) to $\xi = 1/\Delta q \approx 1$ nm, with a distance of the molecules within the columns of 0.38 nm the correlation reaches over about three molecules.[36]

It is also noteworthy that the isotropization temperatures of all compounds are about 60–150 °C lower than those for the previously reported structurally similar PBIs with dodecyloxy side chains.[17b,21] This relates well to the lower binding constants observed for aggregate formation in solution and indicates smaller cohesive forces between the π–π-stacked molecules. Also the substituents at the bay area have an effect on the clearing point. Thus, the isotropization temperature of the tetrachloro-substituted dye **3a** (110 °C) is about 190 °C lower than that of the unsubstituted PBI **6** (304 °C)[22b] with the same imide substituents. Considering 200 °C as an upper limit for the use of flexible plastic substrates in device fabrication,[37] the compounds **3a**, **d**, and **e** are very promising for such applications because they possess relatively low isotropization temperatures in the range of 110–160 °C.

Furthermore, UV/Vis and photoluminescence studies were carried out for LC thin films of these dyes. As shown in Figure 9, the UV/Vis spectrum of a solution-cast thin film of dye **3a** displayed an absorption maximum at 493 nm with two less intense absorption bands at around 533 and 414 nm, respectively. However, no fluorescence could be observed for this thin film. Upon annealing at 105 °C, the sample transformed into the LC phase according to the morphological changes under the optical polarizing microscope (cp. also DSC, Figure 6a) and pronounced spectral changes occurred (the optical textures of the thin films corresponding to the spectra in Figure 9a are shown in Figure S7 in the Supporting Information). Thus, the absorption maximum for the LC phase appeared now at 537 nm which is bathochromically shifted by 44 nm with respect to the pristine state. Concomitantly, the initially non-fluorescent thin film became fluorescent upon annealing. The fluorescence spectrum shows an emission maximum at 554 nm with well-resolved vibronic structure and has a nearly identical lineshape with that observed for aggregates of **3a** in MCH, but with a bathochromic shift of 9 nm. The different optical properties of the solution-cast and annealed thin films of **3a** reflect the different packing feature of **3a** molecules in pristine state and LC phase.

In the case of phenoxy-substituted dyes **3b** and **e**, only one phase below the isotropization point can be observed by DSC measurements. Thus, the solution-cast thin films of these compounds are in LC state. For **3b**, the emission spectrum of the thin film is a mirror image of the S_0–S_1 absorption band with a Stokes shift of 32 nm. In comparison with the dimer spectra in MCH, the spectra in thin film are slightly bathochromically shifted. For dye **3e**, the lineshape of absorption spectrum of the thin film is highly comparable with that of the dimer, apart from a bathochromic shift of about 35 nm. In the fluorescence spectrum of the thin film of **3e**, a broad red-shifted band around 680 nm was ob-

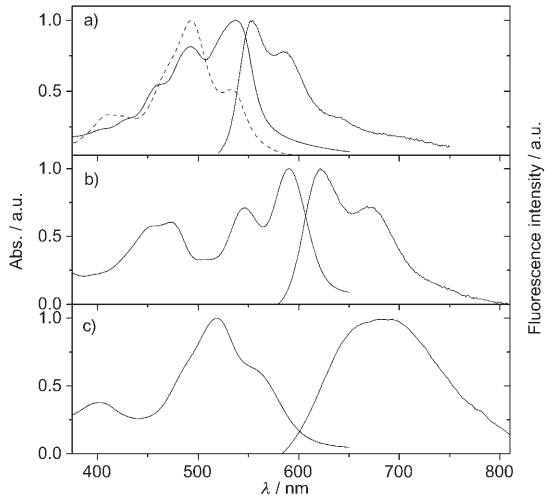

Figure 9. a) Normalized UV/Vis absorption spectrum of the thin film of **3a** cast from MCH solution (dashed line) together with the UV/Vis absorption and fluorescence spectra of the LC thin film (after annealing, solid lines). b) Normalized UV/Vis absorption and fluorescence spectra of the thin film of **3b** cast from MCH solution. c) Normalized UV/Vis absorption and fluorescence spectra of the thin film of **3e** cast from MCH solution.

served, which was about 35 nm bathochromically shifted with respect to that observed in MCH solution.

For the dibromo-substituted dye **3d**, despite the existence of a crystal-LC transition, no spectral changes can be observed in the thin film cast from MCH solution upon annealing. The UV/Vis spectrum displays a λ_{max} at 483 nm with a lower energy band at 540 nm (Figure S8 in the Supporting Information). The thin film is weakly fluorescent with an emission maximum at 624 nm. The observation of broad emission bands of the thin film of **3d**, **e** with very large Stokes shifts (>140 nm) and the fact that no fine structure, in contrast to that of dyes **3a**, **b**, was observed clearly indicate that the π–π stacking of the dyes **3d**,**e** is distinct from that of **3a**,**b** in the LC state.

Discussion

Here we will discuss elaborately some of our pertinent results presented in the preceding sections. The concentration-dependent UV/Vis spectroscopic studies and VPO measurements have clearly shown that the present bay-substituted PBIs **3a**–**f** favorably aggregate to give π–π-stacked dimers in MCH at millimolar concentrations. By contrast, at bay area unsubstituted PBI **6** formed extended oligomeric π–π stacks under comparable conditions according to our recent investigation.[22] This distinct aggregation behavior of at bay area substituted versus unsubstituted PBIs can be explained in terms of their quite different molecular geometry. X-ray crystallographic analysis showed that the π system of unsubstituted PBIs is perfectly planar,[38a,b] while the perylene cores of bay-substituted derivatives, which contain the same bay substituents as the present dyes **3a**–**d**, are significantly distorted.[17,23,38b–d] Depending on the number and steric demand of the substituents, twist angles (θ) of 24 to 37° were found in the solid state for bay-substituted PBIs. To our knowledge, crystal structures for diphenoxy-, dipentafluorophenoxy-, and dipyrrolidinyl-substituted PBIs are not reported in literature. However, as twist angles assessed by semiempirical AM1 calculations for the other four compounds agree well with those determined by X-ray analysis (see Table 5), these values can be estimated with high fidelity.

Table 5. Experimental and calculated twist angles of bay-substituted PBIs.

Structure	Bay substituents	θ [°][a]	θ [°][b]
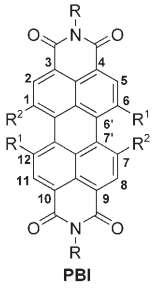	without substituents	0[38a,b]	0
	1,7-diphenoxy	[c]	15
	1,7-dipentafluorophenoxy	[c]	18
	1,7-dibromo	24[23]	24
	1,7-dipyrrolidinyl	[c]	25
	1,6,7,12-tetrachloro	37[17a]	36
	1,6,7,12-tetraphenoxy	25[38b–d]	27

PBI

[a] Twist angle (dihedral angle associated with the 4 carbon atoms C6-C6′-C7′-C7) in the perylene core determined by single crystal X-ray analysis. [b] Calculated by semiempirical AM1 method (CAChe 5.0). [c] Data not available.

The different aggregation behavior of planar and core-twisted PBI dyes, that is, formation of π–π-stacked dimers versus extended π–π stacks, respectively, is a consequence of different intermolecular interactions originating from distinct geometry. In flat PBI **6** monomer, the two π surfaces are equal with respect to the approach of another molecule from the top or bottom face to form dimers and the dimers have the same feature as the monomers, thus, extended aggregates can be formed. However, this situation is changed when the molecular plane is twisted due to the substituents at bay area. For example, the structure of dipyrrolidinyl-substituted PBI obtained from molecular modeling shows that the two substituents point toward the same side of the molecular plane (Figure 10a), making the two π-surfaces of the molecule distinct. One side is sterically much more encumbered than the other side due to the bay substituents. Thus, in the self-assembly process the two sterically less hindered faces of the molecules stack together to form an energy-minimized dimeric unit through larger π–π overlap and to minimize the energy of the system. Indeed, such dimeric units are found in the crystal structure of compound **4**.[23] As revealed by this structure, a rotational displacement around the stacking axis may reduce the steric congestion of the substituents and enforce the π–π contact (Figure 10b). Further aggregation of such dimeric units should be disfavored due to the steric hindrance of the bulky substituents at the accessible π faces. Accordingly, the dimerization of bay-substituted PBI dyes in solution is favored with respect to further aggregation.

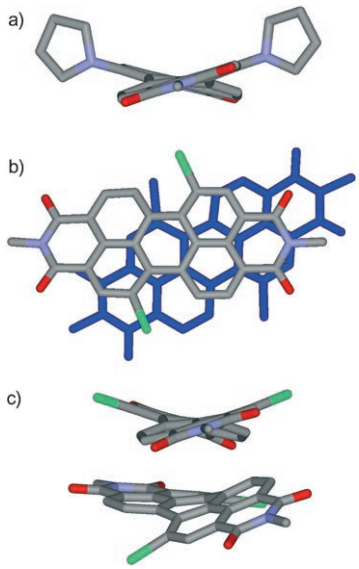

Figure 10. a) Molecular structure of dipyrrolidinyl-substituted PBI (view along the *N*–*N* axis) obtained from molecular modeling. b) Top view of the dimeric unit of compound **4** in crystal structure with a rotational displacement of about 35°. c) Side view of the dimeric unit of compound **4** in crystal structure.[23]

Our results have shown that the aggregation constants of the bay-substituted PBI dyes are 2–4 orders of magnitude smaller than those of the corresponding unsubstituted dyes with the same imide substituents. This can be attributed to the reduced π–π interaction energy in the case of bay-substituted PBIs due to the twisting of the perylene core. Indeed, a good correlation between the twist angle and the Gibbs free energy of π–π stacking, except for **3c**, was observed (Figure 11). Upon increasing the twist angle from 0° for the unsubstituted PBI **6** to the 37° for the tetrachloro-substituted PBI **3a**, the aggregation constant decreased strongly. Thus, the degree of twisting has a pronounced effect on PBI dye aggregation through π–π interaction. The rather good correlation between $\Delta G°$ and θ, despite the different bay-substituents, indicates that the magnitude of $\Delta G°$ mainly depends on the geometry of the perylene bisimide core and the respective bay substituents have only a minor effect on the π–π stacking energy (with the exception of **3c**). This is a reasonable result because for aggregates of twisted π systems we have to expect either an increased distance between the π planes (as observed in the LC phases of **3b**,**d**) or a pronounced displacement between the dyes leading to a smaller π–π contact area (as observed in the LC phase of **3a**).

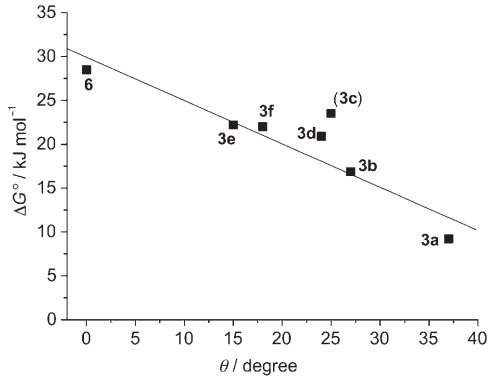

Figure 11. Plot of the Gibbs dimerization energy $\Delta G°$ against the twisting angle θ of the bay-substituted PBIs **3a**–**f** and **6** obtained from calculation (Table 5).

Indeed, the core twisting of these PBIs has significant effect on the molecular packing in the LC phase. Dye **3a** with the largest twist angle (37°) formed a Col_{ro} phase, while for the less distorted dyes **3b** (27°) and **3d** (24°), Col_{ho} phases were observed. The diphenoxy-substituted **3e** (twist angle 15°) and the planar PBI **6** showed a Col_{hd} phase. Thus, obviously, in the case of less twisted dyes, the intracolumnar order decreases and the lattice structure changes from rectangular to hexagonal. A pronounced distortion of the skeleton interferes with the translational and rotational fluctuation of the molecules in the columns and thereby increases the ordering within the columns, which is also reflected in the optical texture of the LC phases of such dyes (Figure 7) as for **3a** and **b** lancet-like domains were observed, while for **3d** and **e**, spherulitic textures were observed. For dye **3a**, the rotational displacement of the dye molecules, that is a prerequisite for the formation of a hexagonal lattice is hindered, due to the bulky chlorine atoms. In contrast, these dyes stack on top of each other with longitudinal offsets along the long molecular axis to form a rectangular phase (Figure 12). With four bulky phenoxy substituents the core of **3b** is nearly disk-like. Taking into account a tilt of the molecular cores with respect to the columnar axis as found for the analogous compound with alkoxy side chains,[21] rotational disorder is not necessarily needed (even if possible to some extent) to form columns with a circular cross-section. Conversely, such a rotational displacement is necessary for the PBI molecules **3d** and **e** to compensate the considerably differing dimensions of the long and short axis of the molecules.[39] This assumption is supported by the observation of identical column diameters for the dyes **3d** and **e**, although the bay substituents in these compounds are quite different (dibromo for **3d** and diphenoxy for **3e**). For the crystal structure of dibromo-substituted PBI **4**,[23] a rotational displacement of about 35° (Figure 10b) between the long axis of the molecules was observed, implying that such displacement could be also feasible in the LC state of disubstituted PBIs.

The twisted π core not only plays a decisive role for the structure and thermodynamic stability of π–π-aggregated PBIs, but it has also a strong effect on the excited state properties of PBI aggregates. For all the present dyes, bathochromic shifts of the aggregate emission bands with respect to monomer emission were observed, indicating a lowering energy of the emissive aggregate state compared to the monomer species. The reduction of the energy can be quantified by the spectroscopic energy difference $\Delta\nu$ (in wavenumbers) between the monomer (0–0) emission maximum and

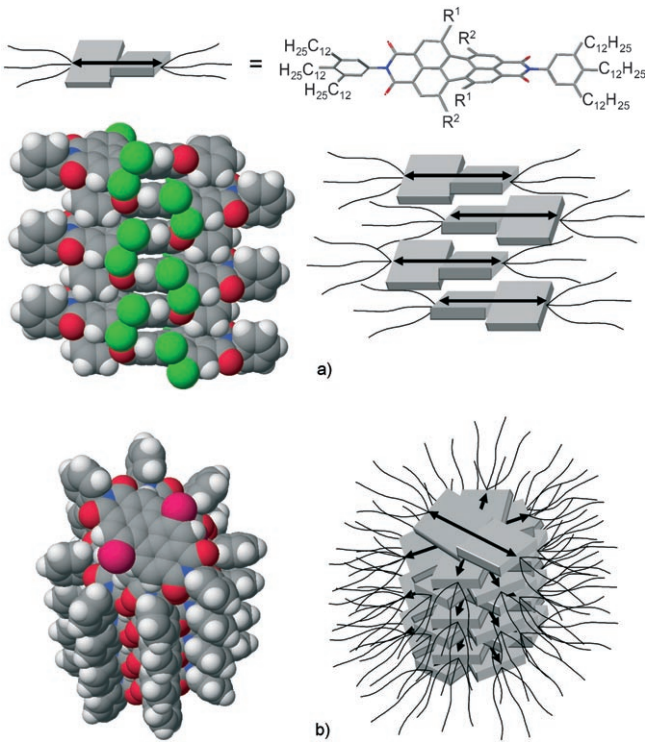

Figure 12. Schematic representation of the proposed packing patterns and the orientation of the transition dipole moments in columnar LC phases of the core-twisted PBI dyes: a) *J*-type π–π stacking of **3a**, and b) cofacial π–π stacking of **3d**,**e**.

the maximum of the aggregate emission band (a quantity introduced to estimate the stabilization energy for excimers[40]). As shown in Figure 13, this energy difference $\Delta\nu$ is highly dependent on the twist angle θ. The planar dye **6** exhibits the largest $\Delta\nu$ value with a bathochromic shift of 4600 cm^{-1}.[22] Upon twisting of the perylene skeleton the $\Delta\nu$ value decreases approximately linearly, despite different electronic properties of the bay substituents. For the dyes **3e** and **f** bearing only two phenoxy substituents at the perylene core, the bathochromic shift is still very significant while it is of minor importance for the dyes with four bay substituents. For instance, the value $\Delta\nu = 309$ cm^{-1} for **3a** is smaller than

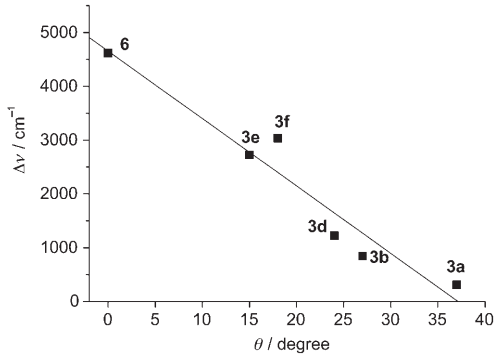

Figure 13. Plot of the energy difference $\Delta\nu$ (in wavenumbers) between the 0–0 emission band of the monomeric dyes and the emission maxima of the aggregated dyes in MCH versus the core twisting angle θ.

the value of the Stokes shift between the absorption and emission maximum (875 cm^{-1}). Accordingly, we can conclude that the energetic relaxation process in the excited state is not significantly more pronounced in dimer aggregates of the distorted dyes **3a**, **b** than for their monomeric species. On the other hand, an explanation is requested for the very significant stabilization of the excited state in the case of dimer aggregates of the more flat derivatives **3e** and **f**.

The above suggested π–π-stacking pattern of the core-twisted dyes in their LC phase and the observed UV/Vis spectroscopic features of π-stacked dyes in solution and thin film can be rationalized by molecular exciton theory.[41] Based on this theory, excitonic coupling between closely stacked chromophores causes changes in the optical spectra as observed for various types of dyes, including PBIs. It has been pointed out that either hypsochromic or bathochromic shifts of the absorption maximum with respect to that of the monomer can occur depending on the stacking geometry and the selection rule for the respective optical transitions. In the most simple case, when two dyes are stacked on top of each other with parallel transition dipole moments only one out of two excitonic transitions is allowed. In most cases, this is the transition to the higher energy state (corresponding to a hypsochromically shifted, that is, *H*-type band) and only in rare cases of pronounced longitudinal displacements between the two dyes it is the transition to the lower energy state (corresponding to the bathochromically shifted *J*-type band).[42] On the other hand, when the transition dipoles are rotationally displaced both bathochromically and hypsochromically shifted bands can be observed.[41] This situation has been observed for the vast majority of aggregates of unsubstituted PBIs and recently elucidated by calculated spectra for a variety of possible geometries based on molecular exciton theory.[25]

In contrast to the parent flat PBIs, for **3a** and **b** only small bathochromic shifts and only minor changes in the band shape were observed upon aggregation in the concentration-dependent UV/Vis spectra in MCH. Both observations imply that the excitonic couplings are weak in the dimers. This is a reasonable result because these twisted π cores cannot approach into close proximity for steric reasons. In addition, according to the packing model in Figure 12a, the longitudinal displacement is characterized by a slipping angle close to the magic angle 54.7°. Accordingly, the electronic coupling remains small for these dye aggregates.[41] In contrast, significantly stronger excitonic coupling effects are observed for the aggregates of the less twisted dye **3c**–**f**. The most evident features of their spectra are hypsochromically shifted absorption maxima in concentration-dependent UV/Vis spectra in MCH and in LC phases that is, however, accompanied with the simultaneous occurrence of another absorption band or at least a shoulder at longer wavelengths (Figure 3 and Figure S1–2 in the Supporting Information). This pattern is indicative of cofacial-type dimers of these dyes with rotational displacements among the long molecular axis.[25,41]

Whilst calculations based on the excitonic coupling theory could successfully describe the spectral changes arising in the UV/Vis absorption spectra for flat PBI upon dimer aggregate formation,[25] they cannot explain the far more pronounced bathochromic shifts in the fluorescence spectra that are observed for the flat PBI **6**[22a] or the slightly twisted PBIs **3c**–**f**. Because these fluorescence spectra exhibit many features that are typically observed for excimers,[28] that is, a pronounced bathochromic shift and a structureless broad band, we suggest that a major structural reorganization process takes places in these dimer aggregates from the original Franck-Condon excited state to the final energetically relaxed state from which emission occurs. Most likely, the π–π distance is reduced in this relaxed state and, thus the electronic coupling between the two dyes is increased. Because the radiative transition from such an excited state leads to an energetically unfavorable state on the ground state potential surface, the fluorescence spectra resemble those observed for excimers.[28] Therefore, even that the dimeric species of PBIs **3c**–**f** are stable in the ground state, bathochromically shifted broad and structureless emission bands are observed for these dyes.

A very interesting phenomenon is the "switch on" of the fluorescence of compound **3a** during the transition from the pristine phase into the LC phase upon annealing. This is indicative for a process, in which the chromophore packing is changed to a *J*-type geometry (Figure 12a) with transition dipole moments parallel.[42] In the pristine thin film, the dye molecules may stack in a more *H*-type geometry where the lowest energy transition is forbidden and accordingly no fluorescence is observed.[42] Upon phase transition, the dyes are slipped into a more longitudinally displaced geometry (Figure 12a), leading to the formation of luminescent *J*-type aggregates. It is noteworthy that such spectral changes might be of interest for various applications, for example, to record the thermal history of material or to inscribe information into a recording medium (e.g., CD-ROM) by the thermal effect of laser light. Similarly, dye **3b** also exhibits the features of a *J*-type packing in the LC phase according to the UV/Vis absorption and fluorescence spectra of the LC thin film in Figure 9. On the other hand, thin LC films of **3d**,**e** show both higher and lower energy bands where the higher energy bands possess the larger oscillator strengths (Figure 9c and Figure S8 in the Supporting Information). This is in good agreement with our packing model that suggests rotational displacements between the transition dipoles. In such columnar π–π stacks, a pronounced relaxation process of the excited state may occur as suggested by the large Stokes shifts and excimer-type emissions of these two dyes. Interestingly, stacking by rotational displacement seems to be more favored by the less twisted disubstituted PBIs than by the strongly twisted tetrasubstituted dyes, which prefer a longitudinal offset giving rise to *J*-type spectra. Although only few examples of the screw-type stacking were observed in the crystal structures of PBIs,[38b] rotational displacements play an important role in the packing of these dyes in LC phases as observed here for **3d**,**e** and previously for unsubstituted PBIs.[21,22]

Conclusion

A series of new, highly photoluminescent core-twisted PBI dyes were synthesized that bear trialkylphenyl groups at the imide positions and two or four substituents at bay area. These compounds are characterized by distortions of the perylene planes with dihedral angles in the range of 15–40° according to crystallographic data and molecular modeling studies. In contrast to the extended oligomeric π stacks formed for planar unsubstituted PBIs, aggregation of this family of dyes was limited to π–π-stacked dimers in apolar solvent due to the distorted aromatic core. Upon excitation of these solutions, fluorescence was observed for the dimer aggregates of all these compounds. Even in condensed state, several PBIs exhibit luminescence as well as mesophase properties, that is, they form thermotropic columnar liquid crystal phases. The core twisting has a significant effect on the π–π-stacking mode of the molecules in solution and in the columnar stacks of the LC phases. In both cases, the more twisted tetrasubstituted dyes prefer longitudinally slipped stacks of the dyes with *J*-type emissive properties, whilst for the less twisted disubstituted dyes, the feature of rotational displacement between the molecules in cofacial aggregates was confirmed. A remarkable linear relationship between the dihedral angle and the ground state dimerization Gibbs free energy as well as the bathochromic shift of the aggregate emission band has been found. The relationship between the degree of distortion of the aromatic core and its self-assembly properties demonstrated here for these PBIs provides useful information for the supramolecular control of electronic and optical properties of aggregates of this type of functional dyes. Possessing high fluorescence quantum yields, low isotropization temperatures, n-type semiconducting and unique self-assembly properties, these dyes are promising materials for organic electronics.

Experimental Section

Materials and methods: 1,7-Dipyrrolidinylperylene-3,4:9,10-tetracarboxylic acid bisanhydride (**1c**) was synthesized by the procedures described previously.[23] 1,7-Dibromoperylene-3,4:9,10-tetracarboxylic acid bisanhydride (**1d**) was synthesized by saponification of isomer-free *N*,*N*′-dicyclohexyl-1,7-dibromo PBI **4**. NMR spectra were recorded at 300 K on Bruker 400 MHz or 600 MHz spectrometers by using TMS ($\delta = 0.0$) as internal standard. The solvents for spectroscopic studies were of spectroscopic grade and used as received. UV/Vis spectra were measured on Lambda 40P spectrometer equipped with a Peltier System as the temperature controller. The vapor pressure osmometry (VPO) measurements were performed on a Knauer osmometer with a universal temperature measurement unit. Benzil was used as standard and a calibration curve in terms of *R* in Ohm versus molal osmotic concentration (moles per kg MCH) was constructed up to 0.01 molal. DSC measurements were performed using a TA Q1000 calorimeter with a heating/cooling rate of 10 °C min^{-1}. At least two heating–cooling cycles were performed for each compound. Optical textures of the LC phases at crossed polarizers were obtained with an Olympus BX-41 polarization microscope equipped with a Linkam THMS 600 hot stage and a temperature controller unit.

X-ray diffraction of LC: Powder X-ray investigations were carried out with a Guinier film camera (Huber Diffraktionstechnik, Germany). Sam-

ples were kept in glass capillaries with a diameter of 1 mm (exception: sample of **3b** on a Be plate) in a temperature-controlled heating stage, quartz-monochromatized $Cu_{K\alpha}$ radiation was used (30 to 60 min exposure time, calibration with the powder pattern of $Pb(NO_3)_2$). 2D patterns were recorded for aligned samples on a glass plate on a temperature-controlled heating stage (alignment at the sample/glass or sample/air interface) with a 2D detector (HI-STAR, Siemens) using $Cu_{K\alpha}$ radiation monochromatized by a Ni filter.

Fluorescence measurements: The steady state fluorescence spectra were recorded on a PTI QM4/2003 spectrofluorometer. The fluorescence quantum yields were determined by optical dilute method.[43] Fluorescein ($\Phi_{fl}=0.92$ in 1*N* aqueous NaOH, for **3a**, **d**), cresyl violet ($\Phi_{fl}=0.54$ in MeOH, for **3c**) and *N*,*N*′-di(2,6-diisopropylphenyl)-1,6,7,12-tetraphenoxyperylene-3,4:9,10-tetracarboxylic acid bisimide ($\Phi_{fl}=0.96$ in $CHCl_3$, for **3b**, **e**, **f**) were used as references. The given quantum yields are averaged from values measured at three different excitation wavelengths.

1,7-Dibromoperylene-3,4:9,10-tetracarboxylic acid bisanhydride (1d): *N*,*N*′-Dicyclohexyl-1,7-dibromoperylene-tetracarboxylic acid bisimide (140 mg, 0.20 mmol), KOH (1.0 g, 18 mmol) was mixed with water (0.5 mL) and *t*BuOH (20 mL). The reaction mixture was stirred at 90 °C for 18 h and the color of the solution became bright green. After cooling to room temperature, the reaction mixture was poured into acetic acid (50 mL) and allowed to stay over night. Then the precipitate was collected by centrifugation and dried in vacuum. The resulting red solid was dissolved in H_2SO_4 (15 mL) and this solution was slowly added into water (100 mL). The precipitate was collected by filtration and washed with large amount of water, and dried in vacuum at 100 °C for 24 h to give a deep red powder (96 mg, 90 %). The purity of this material was enough for further reaction. ^{1}H NMR (600 MHz, D_2SO_4, 300 K, external TMS): $\delta=9.65$ (d, 2H, $J=8.3$ Hz, H_{pery}), 8.98 (s, 2H, H_{pery}), 8.76 (d, 2H, $J=8.4$ Hz, H_{pery}); MS (EI, 70 eV): *m*/*z* (%): 549.8 (100) $[M]^+$, 505.8 (36) $[M-CO_2]^+$, 469.9 (6.4) $[M-Br]^+$.

***N*,*N*′-Di(3,4,5-tridodecylphenyl)-1,6,7,12-tetrachloroperylene-3,4:9,10-tetracarboxylic acid bisimide (3a)**: 1,6,7,12-Tetrachloroperylene- 3,4:9,10-tetracarboxylic acid bisanhydride (0.13 g, 0.24 mmol), 3,4,5-tridodecylaniline (0.30 g, 0.50 mmol) and zinc acetate (0.055 g, 0.30 mmol) were mixed in quinoline (15 mL). The reaction mixture was stirred at 180 °C for 2 h. After cooling to room temperature, the mixture was poured into MeOH (30 mL). The precipitate was collected by filtration, washed with methanol, and then dried in vacuum. The crude product was further purified by silica gel column chromatography (CH_2Cl_2) and then slowly precipitated from CH_2Cl_2/methanol 1:1. The product was isolated as an orange powder by filtration (210 mg, 52 %). ^{1}H NMR (400 MHz, $CDCl_3$, 300 K, TMS): $\delta=8.72$ (s, 4H, H_{pery}), 6.93 (s, 4H, Ar-H), 2.67 (m, 12H, Ar-CH_2), 1.8–1.2 (m, 120H, CH_2),0.88 (m, 18H, CH_3); MS (FAB, matrix: *p*-octyloxynitrobenzene): *m*/*z*: calcd for $C_{108}H_{158}Cl_4N_2O_4$: 1687.1; found 1687.1 $[M]^+$; elemental analysis (%) calcd for $C_{108}H_{158}Cl_4N_2O_4$: C 76.74, H 9.42, N 1.66, Cl 8.39; found: C 76.76, H 9.38, N 1.60, Cl 8.52; UV/Vis (CH_2Cl_2): λ_{max} (ε) = 523 (48100), 490 (33800), 428 (11500 $M^{-1}cm^{-1}$); fluorescence (CH_2Cl_2): $\lambda_{max}=543$ nm; fluorescence quantum yield: $\Phi_{fl}=0.03$.

***N*,*N*′-Di(3,4,5-tridodecylphenyl)-1,6,7,12-tetra(4-*tert*-butylphenoxy)perylene-3,4:9,10-tetracarboxylic acid bisimide (3b)**: Prepared from 1,6,7,12-tetra(4-*tert*-butylphenoxy)perylene-3,4:9,10-tetracarboxylic acid bisanhydride (0.15 g, 0.15 mmol), 3,4,5-tridodecylaniline (0.19 g, 0.31 mmol) and zinc acetate (0.033 g, 0.18 mmol). According to the procedure described above for compound **3a**. A dark-red viscous substance was obtained (170 mg, 53 %). ^{1}H NMR (400 MHz, $CDCl_3$, 300 K, TMS): $\delta=8.22$ (s, 4H, H_{pery}), 7.23 (d, 8H, $J=10.7$ Hz, Ar-H), 6.86 (m, 12H, Ar-H), 2.58 (m, 12H, Ar-CH_2), 1.8–1.2 (m, 156H), 0.88 (m, 18H, CH_3); MS (FAB, matrix: *p*-octyloxynitrobenzene): *m*/*z*: calcd for $C_{148}H_{210}N_2O_8$: 2143.6; found 2143.7 $[M]^+$; elemental analysis (%) calcd for $C_{148}H_{210}N_2O_8$: C 82.86, H 9.87, N 1.31; found: C 82.70, H 9.94, N 1.35; UV/Vis (CH_2Cl_2): λ_{max} (ε) = 580 (50100), 541 (31400), 453 (17400), 267 (51600 $M^{-1}cm^{-1}$); fluorescence (CH_2Cl_2): $\lambda_{max}=611$ nm; fluorescence quantum yield: $\Phi_{fl}=0.95$.

***N*,*N*′-Di(3,4,5-tridodecylphenyl)-1,7-dipyrrolidinylperylene-3,4:9,10-tetracarboxylic acid bisimide (3c)**: Prepared from 1,7-dipyrrolidinylperylene-3,4:9,10-tetracarboxylic acid bisanhydride (0.10 g, 0.19 mmol), 3,4,5-tridodecylaniline (0.26 g, 0.43 mmol) and zinc acetate (0.040 g, 0.22 mmol). According to the procedure described above for compound **3a**, a green viscous substance was obtained (210 mg, 65 %). ^{1}H NMR (400 MHz, $CDCl_3$, 300 K, TMS): $\delta=8.55$ (s, 2H, H_{pery}), 8.49 (d, 2H, $J=8.1$ Hz, H_{pery}), 7.79 (d, 2H, $J=8.1$ Hz, H_{pery}), 6.95 (s, 4H, Ar-H), 3.78 (broad, 4H, $H_{Pyrrolidinyl}$), 2.88 (broad, 4H, $H_{Pyrrolidinyl}$), 2.65 (m, 12H, Ar-CH_2), 2.05 (broad, 8H, $H_{Pyrrolidinyl}$), 1.8–1.2 (m, 120H, CH_2), 0.88 (m, 18H, CH_3); MS (FAB, matrix: *p*-octyloxynitrobenzene): *m*/*z*: calcd for $C_{116}H_{176}N_4O_4$: 1689.4; found: 1689.6 $[M]^+$; elemental analysis (%) calcd for $C_{116}H_{176}N_4O_4$: C 82.41, H 10.49, N, 3.31; found: C 83.14, H 10.68, N, 3.29; UV/Vis (CH_2Cl_2): λ_{max} (ε) = 705 (48200), 654 (24600), 435 (18900), 314 (27900 $M^{-1}cm^{-1}$); fluorescence (CH_2Cl_2): $\lambda_{max}=745$ nm; fluorescence quantum yield: $\Phi_{fl}=0.25$.

***N*,*N*′-Di(3,4,5-tridodecylphenyl)-1,7-dibromoperylene-3,4:9,10-tetracarboxylic acid bisimide (3d)**: Prepared from 1,7-dibromoperylene-3,4:9,10-tetracarboxylic acid bisanhydride (0.26 g, 0.47 mmol), 3,4,5-tridodecylaniline (0.60 g, 1.0 mmol) and zinc acetate (0.10 g, 0.55 mmol). According to the procedure described above for compound **3a**, except that $CHCl_3$/*n*-hexane 1:1 was used for chromatography, to give a orange-red powder (350 mg, 44 %). ^{1}H NMR (400 MHz, $CDCl_3$, 300 K, TMS): $\delta=9.54$ (d, 2H, $J=8.1$ Hz, H_{pery}), 8.96 (s, 2H, H_{pery}), 8.76 (s, 2H, $J=8.2$ Hz, H_{pery}), 6.95 (m, 4H, Ar-H), 2.66 (m, 12H, Ar-CH_2), 1.8–1.2 (m, 120H, CH_2), 0.88 (m, 18H, CH_3); MS (FAB, matrix: *p*-octyloxynitrobenzene): *m*/*z*: calcd for $C_{108}H_{160}Br_2N_2O_4$: 1707.1; found: 1707.3 $[M]^+$; elemental analysis (%) calcd for $C_{108}H_{160}Br_2N_2O_4$: C 75.85, H 9.43, N1.64, Br 9.34; found: C 75.90, H 9.38, N 1.58, Br 9.08; UV/Vis (CH_2Cl_2): λ_{max} (ε) = 527 (57800), 491 (39400), 464 (16000), 388 (6800), 269 (36300 $mol^{-1}dm^3cm^{-1}$); fluorescence (CH_2Cl_2): $\lambda_{max}=544$ nm; fluorescence quantum yield: $\Phi_{fl}=0.26$.

***N*,*N*′-Di(3,4,5-tridodecylphenyl)-1,7-di(4-*tert*-butylphenoxy)perylene-3,4:9,10-tetracarboxylic acid bisimide (3e)**: Compound **3d** (0.10 g, 0.058 mmol), *tert*-butylphenol (0.035 g, 0.23 mmol) and K_2CO_3 (0.030 g, 0.22 mmol) were mixed in anhydrous *N*-methylpyrrolidinone (5 mL). The reaction mixture was stirred at 120 °C for 2 h under argon atmosphere. After cooling to room temperature, MeOH (20 mL) and 1 N HCl (5 mL) was added into the reaction mixture. The precipitate was collected by filtration, washed with methanol, and then dried in vacuum. The crude product was further purified by silica gel column chromatography (CH_2Cl_2) and then precipitated from CH_2Cl_2/methanol 1:1 to give a dark red solid (43 mg, 40 %). ^{1}H NMR (400 MHz, $CDCl_3$, 300 K, TMS): $\delta=$ 9.69 (d, 2H, $J=8.5$ Hz, H_{pery}), 8.65 (d, 2H, $J=8.4$ Hz, H_{pery}), 8.33 (s, 2H, H_{pery}), 7.45 (m, 4H, Ar-H), 7.10 (m, 4H, Ar-H), 6.91 (s, 4H, Ar-H), 2.62 (m, 12H, Ar-CH_2), 1.8–1.2 (m, 138H), 0.88 (m, 18H, CH_3). MS (FAB, matrix: *p*-octyloxynitrobenzene): *m*/*z*: calcd for $C_{128}H_{186}N_2O_6$: 1847.4; found: 1847.6 $[M]^+$; elemental analysis (%) calcd for $C_{128}H_{186}N_2O_6$: C 83.15, H 10.14, N 1.52, found C 82.50, H 10.01, N 1.55; UV/Vis (CH_2Cl_2): λ_{max} (ε) = 546 (56000), 511 (37800), 403 (10567), 268 (49800 $M^{-1}cm^{-1}$); fluorescence (CH_2Cl_2): $\lambda_{max}=575$ nm; fluorescence quantum yield: $\Phi_{fl}=$ 0.87.

***N*,*N*′-Di(3,4,5-tridodecylphenyl)-1,7-di(pentafluorophenoxy)perylene-3,4:9,10-tetracarboxylic acid bisimide (3f)**: Prepared from compound **3d** (0.050 g, 0.029 mmol), pentafluorophenol (0.53 g, 0.23 mmol) and K_2CO_3 (0.36 g, 0.22 mmol). According to the procedure described above for compound **3e**, a deep red solid was obtained (34 mg, 61 %). ^{1}H NMR (400 MHz, $CDCl_3$, 300 K, TMS): $\delta=9.52$ (d, 2H, $J=8.4$ Hz, H_{pery}), 8.75 (d, 2H, $J=8.4$ Hz, H_{pery}), 8.19 (s, 2H, H_{pery}), 6.92 (s, 4H, Ar-H), 2.64 (m, 12H, Ar-CH_2), 1.8–1.2 (m, 120H, CH_2), 0.87 (m, 18H, CH_3); MS (MALDI-TOF, matrix: DTCB): *m*/*z*: calcd for $C_{120}H_{160}F_{10}N_2O_6$: 1915.2; found: 1915.2 $[M]^+$; elemental analysis (%) calcd for $C_{120}H_{160}F_{10}N_2O_6$: C 75.20, H 8.41, N 1.46, found: C 75.31, H 8.63, N 1.47; UV/Vis (CH_2Cl_2): λ_{max} (ε) = 530 (71300), 494 (45300), 465 (17200), 381 (7800 $M^{-1}cm^{-1}$); fluorescence (CH_2Cl_2): $\lambda_{max}=547$ nm; fluorescence quantum yield: $\Phi_{fl}=$ 0.79.

Acknowledgements

We are grateful to the Deutsche Forschungsgemeinschaft for financial support of this work within the research graduate school GK 1221 "Control of electronic properties of aggregates of π-conjugated molecules" and the Fonds der Chemischen Industrie.

[1] a) C. D. Simpson, J. Wu, M. D. Watson, K. Müllen, *J. Mater. Chem.* **2004**, *14*, 494–504; b) F. J. M. Hoeben, P. Jonkheijm, E. W. Meijer, A. P. H. J. Schenning, *Chem. Rev.* **2005**, *105*, 1491–1546; c) *Supramolecular Dye Chemistry, Vol. 258* (Ed.: F. Würthner), *Topics in Current Chemistry*, Springer, Berlin, **2005**.

[2] D. Adam, P. Schuhmacher, J. Simmerer, L. Häussling, K. Siemensmeyer, K.-H. Etzbach, H. Ringsdorf, D. Haarer, *Nature* **1994**, *371*, 141–143.

[3] A. P. H. J. Schenning, F. B. G. Benneker, H. P. M. Geurts, X. Y. Liu, R. J. M. Nolte, *J. Am. Chem. Soc.* **1996**, *118*, 8549–8552.

[4] a) C. F. van Nostrum, S. J. Picken, A.-J. Schouten, R. J. M. Nolte, *J. Am. Chem. Soc.* **1995**, *117*, 9957–9965; b) H. Engelkamp, S. Middelbeek, R. J. M. Nolte, *Science* **1999**, *284*, 785–788.

[5] a) W. Pisula, M. Kastler, D. Wasserfallen, T. Pakula, K. Müllen, *J. Am. Chem. Soc.* **2004**, *126*, 8074–8075; b) J. P. Hill, W. Jin, A. Kosaka, T. Fukushima, H. Ichihara, T. Shimomura, K. Ito, T. Hashizume, N. Ishii, T. Aida, *Science* **2004**, *304*, 1481–1483.

[6] F. Würthner, *Chem. Commun.* **2004**, 1564–1579 and references therein.

[7] P. Gregory, *J. Porphyrins Phthalocyanines* **2000**, *4*, 432–437.

[8] K.-Y. Law, *Chem. Rev.* **1993**, *93*, 449–486.

[9] a) J. Simmerer, B. Glüsen, W. Paulus, A. Kettner, P. Schuhmacher, D. Adam, K.-H. Etzbach, K. Siemensmeyer, J. H. Wendorff, H. Ringsdorf, D. Haarer, *Adv. Mater.* **1996**, *8*, 815–819; b) T. Christ, B. Glüsen, A. Greiner, A. Kettner, R. Sander, V. Stümpflen, V. Tsukruk, J. H. Wendorff, *Adv. Mater.* **1997**, *9*, 48–52; c) H. E. Katz, Z. Bao, S. L. Gilat, *Acc. Chem. Res.* **2001**, *34*, 359–369; d) C. D. Dimitrakopoulos, P. R. L. Malenfant, *Adv. Mater.* **2002**, *14*, 99–117.

[10] a) D. Wöhrle, D. Meissner, *Adv. Mater.* **1991**, *3*, 129–138; b) C. J. Brabec, N. S. Sariciftci, J. C. Hummelen, *Adv. Funct. Mater.* **2001**, *11*, 15–26.

[11] a) A. W. Snow, N. L. Jarvis, *J. Am. Chem. Soc.* **1984**, *106*, 4706–4711; b) C. A. Hunter, J. K. M. Sanders, *J. Am. Chem. Soc.* **1990**, *112*, 5525–5534; c) A. J. Zych, B. L. Iverson, *J. Am. Chem. Soc.* **2000**, *122*, 8898–8909; d) Apperloo, R. A. Janssen, P. R. L. Malenfant, J. M. J. Fréchet, *Macromolecules* **2000**, *33*, 7038–7043; e) L. J. J. Brunsveld, H. Zhang, M. Glasbeek, J. A. J. M. Vekemans, E. W. Meijer, *J. Am. Chem. Soc.* **2000**, *122*, 6175–6182; f) J. Wu, A. Fechtenkotter, J. Gauss, M. D. Watson, M. Kastler, C. Fechtenkotter, M. Wagner, K. Müllen, *J. Am. Chem. Soc.* **2004**, *126*, 11311–11321; g) T.-Q. Nguyen, R. Martel, R. Avouris, M. L. Bushey, L. Brus, C. Nuckolls, *J. Am. Chem. Soc.* **2004**, *126*, 5324–5242; h) M. J. Fuller, L. E. Sinks, B. Rybtchinski, J. M. Giaimo, X. Li, M. R. Wasielewski, *J. Phys. Chem. A* **2005**, *109*, 970–975.

[12] a) A. Ajayaghosh, S. J. George, *J. Am. Chem. Soc.* **2001**, *123*, 5148–5149; b) K. Sugiyasu, N. Fujita, S. Shinkai, *Angew. Chem.* **2004**, *116*, 1249–1253; *Angew. Chem. Int. Ed.* **2004**, *43*, 1229–1233; c) F. Würthner, B. Hanke, M. Lysetska, G. Lambright, G. S. Harms, *Org. Lett.* **2005**, *7*, 967–970.

[13] a) A. N. Cammidge, R. J. Bushby in *Handbook of Liquid Crystals, Vol. 2B, Low Molecular Weight Liquid Crystals II* (Eds.: D. Demus, J. Goodby, G. W. Gray, H.-W. Spiess, V. Vill), Wiley-VCH, Weinheim, **1998**, pp. 693–743; b) S. Chandrasekhar in *Handbook of Liquid Crystals, Vol. 2B, Low Molecular Weight Liquid Crystals II* (Eds.: D. Demus, J. Goodby, G. W. Gray, H.-W. Spiess, V. Vill), Wiley-VCH, Weinheim, **1998**, pp. 749–777; c) S. Chandrasekhar, B. K. Sadashiva, K. A. Suresh, *Pramana* **1977**, *9*, 471–480; d) Z. Ali-Adib, G. J. Clarkson, N. B. Mckeown, K. E. Treacher, H. F. Gleeson, A. S. Stennett, *J. Mater. Chem.* **1998**, *8*, 2371–2378; e) B. R. Patel, K. S. Suslick, *J. Am. Chem. Soc.* **1998**, *120*, 11802–11803; f) S. Benning, H.-S. Kitzerow, H. Bock, M.-F. Achard, *Liq. Cryst.* **2000**, 901–906; g) U. Rohr, C. Kohl, K. Müllen, A. van de Craats, J. Warman, *J. Mater. Chem.* **2001**, *11*, 1789–1799; h) S.-G. Liu, G. Sui, R. A. Cormier, R. M. Leblanc, B. A. Gregg, *J. Phys. Chem. B* **2002**, *106*, 1307–1315; i) M. Lee, J.-W. Kim, S. Peleshanko, K. Larson, Y.-S. Yoo, D. Vaknin, S. Markutsya, V. V. Tsukruk, *J. Am. Chem. Soc.* **2002**, *124*, 9121–9128.

[14] A. P. H. J. Schenning, E. W. Meijer, *Chem. Commun.* **2005**, 3245–3258.

[15] a) J. M. Warman, A. M. Van De Craats, *Mol. Cryst. Liq. Cryst.* **2003**, *396*, 41–72; b) J. M. Warman, M. P. de Haas, G. Dicker, F. C. Grozema, J. Piris, M. G. Debije, *Chem. Mater.* **2004**, *16*, 4600–4609.

[16] M. G. Debije, J. Piris, M. P. de Haas, J. M. Warman, Ž. Tomović, C. D. Simpson, M. D. Watson, K. Müllen, *J. Am. Chem. Soc.* **2004**, *126*, 4641–4645.

[17] a) Z. Chen, M. G. Debije, T. Debaerdemaeker, P. Osswald, F. Würthner, *ChemPhysChem* **2004**, *5*, 137–140; b) M. G. Debije, Z. Chen, J. Piris, R. B. Neder, M. M. Watson, K. Müllen, F. Würthner, *J. Mater. Chem.* **2005**, *15*, 1270–1276.

[18] S. Xiao, M. Myers, Q. Miao, S. Sanaur, K. Pang, M. L. Steigerwald, C. Nuckolls, *Angew. Chem.* **2005**, *117*, 7556–7560; *Angew. Chem. Int. Ed.* **2005**, *44*, 7390–7394.

[19] a) D. Schlettwein, D. Wöhrle, E. Karmann, U. Melville, *Chem. Mater.* **1994**, *6*, 3–6; b) G. Horowitz, F. Kouki, P. Spearman, D. Fichou, C. Nogues, X. Pan, F. Garnier, *Adv. Mater.* **1996**, *8*, 242–244; c) C. W. Struijk, A. B. Sieval, J. E. J. Dakhorst, M. Dijk, P. Kimkes, R. B. M. Koehorst, H. Donker, T. J. Schaafsma, S. J. Picken, A. M. van de Craats, J. M. Warman, H. Zuilhof, E. J. R. Sudhölter, *J. Am. Chem. Soc.* **2000**, *122*, 11057–11066; d) P. R. L. Malenfant, C. D. Dimitrakopoulos, J. D. Gelorme, L. L. Kosbar, T. O. Graham, A. Curioni, W. Andreoni, *Appl. Phys. Lett.* **2002**, *80*, 2517–2519; e) B. A. Jones, M. J. Ahrens, M.-H. Yoon, A. Facchetti, T. J. Marks, M. R. Wasielewski, *Angew. Chem.* **2004**, *116*, 6523–6526; *Angew. Chem. Int. Ed.* **2004**, *43*, 6363–6366.

[20] M. Kastler, W. Pisula, D. Wasserfallen, T. Pakula, K. Müllen, *J. Am. Chem. Soc.* **2005**, *127*, 4286–4296.

[21] F. Würthner, C. Thalacker, S. Diele, C. Tschierske, *Chem. Eur. J.* **2001**, *7*, 2245–2253.

[22] a) F. Würthner, Z. Chen, V. Dehm, V. Stepanenko, *Chem. Commun.* **2006**, 1188–1190; b) Z. Chen, V. Stepanenko, V. Dehm, P. Prins, L. D. A. Siebbeles, J. Seibt, P. Marquetand, V. Engel, F. Würthner, *Chem. Eur. J.* **2006**, *12*, 436–449 (preceding paper).

[23] F. Würthner, V. Stepanenko, Z. Chen, C. R. Saha-Möller, N. Kocher, D. Stalke, *J. Org. Chem.* **2004**, *69*, 7933–7939.

[24] a) R. Gvishi, R. Reisfeld, Z. Burshtein, *Chem. Phys. Lett.* **1993**, *213*, 338–344; b) M. Sadrai, L. Hadel, R. R. Sauers, S. Husain, K. Krogh-Jespersen, J. D. Westbrook, G. R. Bird, *J. Phys. Chem.* **1992**, *96*, 7988–7996.

[25] No considerable difference was found in the theoretically calculated dimer and trimer absorption spectra of PBI **6**. J. Seibt, P. Marquetand, V. Engel, Z. Chen, V. Dehm, F. Würthner, *Chem. Phys.* **2006**, *328*, 354–362.

[26] a) R. B. Martin, *Chem. Rev.* **1996**, *96*, 3043–3064; b) F. Würthner, S. Yao, T. Debaerdemaeker, R. Wortmann, *J. Am. Chem. Soc.* **2002**, *124*, 9431–9447.

[27] E. H. A. Beckers, Z. Chen, S. C. J. Meskers, P. Jonkheijm, A. P. H. J. Schenning, X.-Q. Li, P. Osswald, F. Würthner, R. A. J. Janssen, *J. Phys. Chem. B* **2006**, *110*, 16967–16978.

[28] J. B. Birks, *Rep. Prog. Phys.* **1975**, *38*, 903–974.

[29] C. Tschierske, *J. Mater. Chem.* **1998**, *8*, 1485–1508.

[30] I. Shiyanovskaya, K. D. Singer, V. Percec, T. K. Bera, Y. Miura, M. Glodde, *Phys. Rev. B* **2003**, *67*, 035204/1–035204/7.

[31] The diffuse scattering at $d = 0.48$ nm, associated to the mean distance between the fluid alkyl chains has its maximum on the meridian (see Figure 8b and S6b, Supporting Information). This might indicate some preference of the fluid alkyl chains to be organized parallel to the long axis of the columns, which could be the result of the changed conformational equilibrium due to the direct connection of the alkyl chains to the aromatic cores. A preferred organization of the alkyl chains parallel to the columns would provide a stronger

segregation of alkyl chains and aromatic cores, because in this case a sliding of the molecules parallel to the columns short axes should be restricted. This means that the interfaces between aromatic cores and alkyl chains should become sharper and there is an improved packing of the aromatic cores which (together with the restrictions provided by the twisted conformation of the aromatic cores) should improve the overlapping of the π systems along the columns.

[32] T. Komatsu, K. Ohta, T. Watanabe, H. Ikemoto, T. Fujimoto, I. Yamamoto, *J. Mater. Chem.* **1994**, *4*, 537–540.

[33] In the crystal structure (see ref. [17a]), the intramolecular Cl–Cl distance at the same side of PBI molecule is 3.1 Å and the nearest intermolecular Cl–Cl distance is 4.2 Å. In the LC phase, the Cl atoms could be in close contact and form ribbons that are running parallel to the columns. The Cl-Cl interaction might contribute to the liquid crystallinity of **3a**. Recently, a series of columnar mesophases were reported for indene and pseudoazulene compounds with rigid aromatic core which contain polarisable atoms such as Cl, instead of alky chains, as the soft moieties. See: S. Basurto, S. García, A. G. Neo, T. Torroba, C. F. Marcos, D. Miguel, J. Barberá, M. Blanca Ros, M. R. de la Fuente, *Chem. Eur. J.* **2005**, *11*, 5362–5376.

[34] A. Immirzi, B. Perini, *Acta Crystallogr. Sect. A* **1977**, *33*, 216–218.

[35] V. Percec, C.-H. Ahn, T. K. Bera, G. Ungar, D. J. P. Yeardley, *Chem. Eur. J.* **1999**, *5*, 1070–1083.

[36] J. M. Seddon in *Handbook of Liquid Crystals, Vol. 1* (Eds.: D. Demus, J. Goodby, G. W. Gray, H.-W. Spiess, V. Vill), Wiley-VCH, Weinheim, **1998**, p. 648.

[37] J. Tant, Y. H. Geerts, M. Lehmann, V. De Cupere, G. Zucchi, B. W. Laursen, T. Bjørnholm, V. Lemaur, V. Marcq, A. Burquel, E. Hennebicq, F. Gardebien, P. Viville, D. Beljonne, R. Lazzaroni, J. Cornil, *J. Phys. Chem. B* **2005**, *109*, 20315–20323.

[38] a) G. Klebe, F. Graser, E. Hädicke, J. Berndt, *Acta Crystallogr. Sect. B* **1989**, *45*, 69–77; b) P. Zugenmaier, J. Duff, T. L. Bluhm, *Cryst. Res. Technol.* **2000**, *35*, 1095–1115; c) F. Würthner, A. Sautter, C. Thalacker, *Angew. Chem.* **2000**, *112*, 1298–1301; *Angew. Chem. Int. Ed.* **2000**, *39*, 1243–1245; d) P. Osswald, D. Leusser, D. Stalke, F. Würthner, *Angew. Chem.* **2005**, *117*, 254–257; *Angew. Chem. Int. Ed.* **2005**, *44*, 250–253.

[39] U. Beginn, *Prog. Polym. Sci.* **2003**, *28*, 1049–1105.

[40] a) S. A. Jenekhe, J. A. Osaheni, *Science* **1994**, *265*, 765–768; b) H. Ohkita, S. Ito, M. Yamamoto, Y. Tohda, K. Tani, *J. Phys. Chem. A* **2002**, *106*, 2140–2145.

[41] a) E. D. McRae, M. Kasha, *J. Chem. Phys.* **1958**, *28*, 721–722; b) M. Kasha, H. R. Rawls, M. A. El-Bayoumi, *Pure Appl. Chem.* **1965**, *11*, 371–392; c) V. Czikkely, H. D. Försterling, H. Kuhn, *Chem. Phys. Lett.* **1970**, *6*, 11–14; d) E. C. Evans, Q. Song, P. W. Bohn, *J. Phys. Chem.* **1993**, *97*, 12302–12308; e) B. M. W. Langeveld-Voss, D. Beljonne, Z. Shuai, R. A. Janssen, S. C. J. Meskers, E. W. Meijer, J.-L. Brédas, *Adv. Mater.* **1998**, *10*, 1343–1348; f) J. M. Ribó, J. M. Bofill, J. Crusats, R. Rubires, *Chem. Eur. J.* **2001**, *7*, 2733–2737.

[42] a) P. W. Bohn, *Annu. Rev. Phys. Chem.* **1993**, *44*, 37–60; b) *J-Aggregates* (Ed.: T. Kobayashi), World Scientific, Singapore, **1996**; c) E. S. Emerson, M. A. Conlin, A. E. Rosenoff, K. S. Norland, H. Rodriguez, G. R. Bird, *J. Phys. Chem.* **1967**, *71*, 2396–2403; d) H. Stegemeyer, F. Stöckel, *Ber. Bunsenges. Phys. Chem.* **1996**, *100*, 9–14; e) W. J. Harrison, D. L. Mateer, G. J. T. Tiddy, *J. Phys. Chem.* **1996**, *100*, 2310–2321; f) H. v. Berlepsch, C. Böttcher, A. Ouart, C. Burger, S. Dähne, S. Kirstein, *J. Phys. Chem. B* **2000**, *104*, 5255–5262; g) A. B. Koren, M. D. Curtis, A. H. Francis, J. W. Kampf, *J. Am. Chem. Soc.* **2003**, *125*, 5040–5050.

[43] J. N. Demas, G. A. Crosby, *J. Phys. Chem.* **1971**, *75*, 991–1024.

Received: June 22, 2006
Revised: October 23, 2006
Published online: December 4, 2006

